Non-Enzymatic Synthesis of Bioactive Isoprostanoids in the Diatom *Phaeodactylum* following Oxidative Stress[1]

Josselin Lupette,[a] Antoine Jaussaud,[a] Claire Vigor,[b] Camille Oger,[b] Jean-Marie Galano,[b] Guillaume Réversat,[b] Joseph Vercauteren,[b] Juliette Jouhet,[a] Thierry Durand,[b] and Eric Maréchal[a,2,3]

[a]Laboratoire de Physiologie Cellulaire et Végétale, Unité Mixte de Recherche 5168, Centre National de la Recherche Scientifique, Commissariat à l'Energie Atomique, Institut National de la Recherche Agronomique, Université Grenoble Alpes, Institut de Biosciences Biotechnologies de Grenoble, Commissariat à l'Energie Atomique Grenoble, 38000 Grenoble, France

[b]Institut des Biomolécules Max Mousseron, Unité Mixte de Recherche 5247, Université de Montpellier, Centre National de la Recherche Scientifique, Ecole Nationale Supérieure de Chimie de Montpellier, F-34093 Montpellier cedex 05, France

ORCID IDs: 0000-0002-7842-575X (J.L.); 0000-0002-0755-4140 (A.J.); 0000-0002-0201-1235 (J.V.); 0000-0002-0060-1696 (E.M.)

The ecological success of diatoms requires a remarkable ability to survive many types of stress, including variations in temperature, light, salinity, and nutrient availability. On exposure to these stresses, diatoms exhibit common responses, including growth arrest, impairment of photosynthesis, production of reactive oxygen species, and accumulation of triacylglycerol (TAG). We studied the production of cyclopentane oxylipins derived from fatty acids in the diatom *Phaeodactylum tricornutum* in response to oxidative stress. *P. tricornutum* lacks the enzymatic pathway for producing cyclopentane-oxylipins, such as jasmonate, prostaglandins, or thromboxanes. In cells subjected to increasing doses of hydrogen peroxide (H_2O_2), we detected nonenzymatic production of isoprostanoids, including six phytoprostanes, three F_{2t}-isoprostanes, two F_{3t}-isoprostanes, and three F_{4t}-neuroprostanes, by radical peroxidation of α-linolenic, arachidonic, eicosapentaenoic, and docosahexanoic acids, respectively. H_2O_2 also triggered photosynthesis impairment and TAG accumulation. F_{1t}-phytoprostanes constitute the major class detected (300 pmol per 1 million cells; intracellular concentration, ~4 μM). Only two glycerolipids, phosphatidylcholine and diacylglyceryl-hydroxymethyl-trimethyl-alanine, could provide all substrates for these isoprostanoids. Treatment of *P. tricornutum* with nine synthetic isoprostanoids produced an effect in the micromolar range, marked by the accumulation of TAG and reduced growth, without affecting photosynthesis. Therefore, the emission of H_2O_2 and free radicals upon exposure to stresses can lead to glycerolipid peroxidation and nonenzymatic synthesis of isoprostanoids, inhibiting growth and contributing to the induction of TAG accumulation via unknown processes. This characterization of nonenzymatic oxylipins in *P. tricornutum* opens a field of research on the study of processes controlled by isoprostanoid signaling in various physiological and environmental contexts in diatoms.

Diatoms are an important group of phytoplankton widespread in freshwaters and oceans. In addition to the carbon cycle, in which they are critical for CO_2 capture (Scala and Bowler, 2001), they play significant roles in other geochemical cycles via the biogenic conversion of nitrogen (Dolch et al., 2017; McCarthy et al., 2017) or silica (Benoiston et al., 2017). They are at the base of the aquatic microbial food web and are grazed by copepods and juvenile invertebrates (Buchan et al., 2014). Their ecological success requires a remarkable ability to cope with all types of stress, including biotic interactions with grazers, resistance to physicochemical variations, such as temperature, light, salinity, and nutrient availability, and exposure to a multitude of toxic compounds, including anthropogenic pollutants (Conte et al., 2018). Studies in diatoms have benefited from developments in the model species *Phaeodactylum tricornutum*, whose lipidome has been fully characterized under various stress conditions (Abida et al., 2015).

Common responses in diatoms to a variety of stresses include growth arrest (Abida et al., 2015; Collins et al., 2016; Conte et al., 2018), photosynthesis impairment and activation of photoprotection (Roháček et al., 2014; Taddei et al., 2016), emission of reactive oxygen species (ROS; Allen et al., 2008; Burch and Franz, 2016; Collins et al., 2016), and extensive remodeling of membrane glycerolipids (Abida et al., 2015; Collins et al., 2016; Conte et al., 2018).

[1]This work was supported by a Flagship program from the CEA High Commissioner, a CEA DRF Impulsion program, and "Investissements d'avenir" programs funded by the French National Research Agency (ANR-10-LABEX-04 GRAL Labex, Grenoble Alliance for Integrated Structural Cell Biology; ANR-11-BTBR-0008 Oceanomics and ANR-15-IDEX-02 GlycoAlps).

[2]Author for contact: eric.marechal@cea.fr.

[3]Senior author.

The author responsible for distribution of materials integral to the findings presented in this article in accordance with the policy described in the Instructions for Authors (www.plantphysiol.org) is: Eric Maréchal (eric.marechal@cea.fr).

J.L. performed most of the experiments; A.J. provided technical assistance for phenotypic analyses; C.V., C.O., and T.D performed isoprostanoid analyses; J.L. and J.J. performed glycerolipidome analyses; J.-M.G., G.R., and J.V. contributed to isoprostanoid syntheses and analyses; C.V., J.J., and T.D. provided expertise in the analyses of all results; E.M. conceived the project; all the authors contributed to the writing of the article.

www.plantphysiol.org/cgi/doi/10.1104/pp.18.00925

Some of these general responses are physiologically or metabolically linked, explaining why they are commonly encountered. In particular, photosynthesis impairment is marked by an imbalance between the absorption of light energy and the capacity to use it, leading to the generation of superoxide anion ($O_2^{\bullet-}$) and derivatives, such as hydrogen peroxide (H_2O_2) and hydroxyl radical ($OH^{\bullet}$; Mullineaux et al., 2018). Before oxidative damage to PSII becomes significant, excess excitation energy usually is dissipated safely by antioxidant compounds like carotenoids or by processes acting as electron sinks. One of the energy dissipation processes involves the reduction of oxygen to $O_2^{\bullet-}$ via the Mehler reaction in the water-water cycle and gives rise to H_2O_2 by the action of superoxide dismutases (two genes in the diatom *P. tricornutum*, Phatr3_J12583 and Phatr3_J42832; Curien et al., 2016; Mullineaux et al., 2018). Whereas water-water cycle activity is low in angiosperms, it accounts for up to 49% of total electron flux in diatoms (Warring et al., 2014). ROS chemistry is complex, and species can arise from different parallel routes, such as production of the free radical $OH^{\bullet}$ from H_2O_2 either by interaction with $O_2^{\bullet-}$ via the Heiber-Weiss reaction or by interaction with metal ions via the Fenton reaction (Longini et al., 2017). The free radical $O_2^{\bullet-}$ can be produced not only by chloroplasts but also through mitochondrial electron transfer chain leakage directly to oxygen or by some endomembrane NADPH oxidases. Eventually, H_2O_2 can be generated by a variety of peroxisomal enzymes (Milne et al., 2011; Mullineaux et al., 2018).

The free radical $OH^{\bullet}$ can trigger lipid peroxidation by hydrogen abstraction from polyunsaturated fatty acids (PUFAs) and the addition of molecular oxygen to form a peroxyl radical (Milne et al., 2011; Longini et al., 2017). The produced intermediates can undergo a nonenzymatic series of cyclization, addition of a second molecular oxygen, and reduction to form isoprostanoids (Galano et al., 2017), which are more stable than other peroxidation products, such as aldehydes or peroxyl radicals (Longini et al., 2017).

Therefore, an important interplay between ROS-dependent signaling and glycerolipid status is expected. Glycerolipids consist of a glycerol backbone, esterified at positions *sn*-1 and *sn*-2 to fatty acids (FAs) of various carbon chain lengths and desaturation levels and harboring a polar head or a third FA at position *sn*-3. Glycerolipid classes include (1) phosphoglycerolipids usually present in endoplasmic reticulum and endomembranes, such as phosphatidylcholine (PC); (2) betaine lipids, such as diacylglyceryl-hydroxymethyl-*N*,*N*,*N*-trimethyl-*β*-alanine (DGTA); and (3) plastid glycoglycerolipids, such monogalactosyldiacylglycerol (MGDG) or digalactosyldiacylglycerol (DGDG). When the polar head is substituted by an FA, (4) triacylglycerols (TAGs) are produced and accumulate in lipid droplets. Each of these classes is characterized by a profile of FAs, ranging from medium-chain saturated FAs (e.g. palmitic acid with 16 carbons and no double bonds [16:0]) to very-long-chain (VLC) PUFAs (e.g. eicosapentaenoic acids, with 20 carbons and five double bonds [20:5]; Lupette and Maréchal, 2018). Stress-induced remodeling involves changes in the proportions of glycerolipid classes and, within a class, a tuning of the relative proportions of FAs. Nonstressed diatoms have high levels of VLC-PUFAs, whereas stressed cells accumulate TAG, usually with higher proportions of saturated and monounsaturated FAs (Abida et al., 2015; Dolch et al., 2017; Conte et al., 2018).

When *P. tricornutum* is subjected to acute treatment with 150 μM H_2O_2, changes occur in the proportions of the oxidized forms of FAs, or oxylipins (Collins et al., 2016). However, this analysis did not allow the determination of the precise oxylipin molecular structures for each mass spectrometry peak assigned (Collins et al., 2016). Interestingly, a recent screen for small chemicals triggering TAG accumulation in *P. tricornutum* identified compounds known to interfere with specific oxylipins in animal cells; they included misoprostol, a phosphatidylglycerol (PG) E1 analog, and azapropazone and meloxicam, two prostanoid-signaling modulators acting as potent PG-endoperoxide synthase inhibitors (Conte et al., 2018). This suggests that oxylipins containing a prostane ring (e.g. prostaglandins D–F) or at least a cyclopentane cycle (e.g. jasmonic acids) might be derived from PUFA peroxides, downstream of H_2O_2 treatment, and be associated with lipid remodeling.

Cyclopentane-containing oxylipins are produced via two major routes: enzymatic synthesis and nonenzymatic chemical synthesis (Supplemental Fig. S1). Concerning the first route, in the genome of *P. tricornutum*, we could not detect any homolog of the enzymes classically involved in cyclopentane-oxylipin metabolism in animals (Funk, 2001) or plants (Blée, 1998, 2002; Feussner and Wasternack, 2002; Andreou and Feussner, 2009). Neither could we detect any homolog of enzymes involved in the synthesis of thromboxane (Funk, 2001), which has an ether-containing ring in place of a cyclopentane, or enzymes involved in the synthesis of noncyclic oxylipins in plants (Feussner and Wasternack, 2002). *P. tricornutum*, therefore, lacks the enzymatic equipment to produce cyclopentane-oxylipin and differs from other diatom species, such as *Skeletonema marinoi*, in which enzymatic pathways have been described (Gerecht et al., 2011; Gallina et al., 2016; Di Dato et al., 2017). Therefore, the presence of a high basal level of oxidized FAs (5%–7%) reported in the lipidome of *P. tricornutum* (Collins et al., 2016), with apparently a high structural but unresolved diversity, is puzzling.

The nonenzymatic formation of cyclopentane-oxylipins, isomers of prostanoids, also called isoprostanoids (Morrow et al., 1990), requires the presence of free radicals such as $OH^{\bullet}$ (Mallick and Mohn, 2000; Roy et al., 2017) and the presence of at least three double bonds in the PUFA. PUFA peroxidation occurs in three steps: initiation by the attack of a radical species, propagation, and termination with the intervention of antioxidants (Montuschi et al., 2004). Depending

on the PUFA precursors, different groups of PG-like compounds (i.e. isoprostanes) are generated: phytoprostanes (PhytoPs) from the radical peroxidation of α-linolenic acid (18:3ω3; Parchmann and Mueller, 1998); F_{2t}-isoprostanes (F_{2t}-IsoPs) and F_{3t}-isoprostanes (F_{3t}-IsoPs) from arachidonic acid (20:4ω6) and eicosapentaenoic acid (20:5ω3), respectively (Morrow et al., 1990; Guy et al., 2014); and F_{4t}-neuroprostanes (F_{4t}-NeuroPs) from docosahexaenoic acid (22:6ω3; Nourooz-Zadeh et al., 1998; Roberts et al., 1998; Fig. 1).

In a previously reported mass spectrometry-based profiling of oxidized lipids (Collins et al., 2016), H_2O_2 treatment did not significantly increase the overall proportion of oxidized acyl moieties, but a selective modulation of some peaks was observed and was consistent with a possible modulation of PUFA oxidation, as described in numerous cell models in response to H_2O_2 in both plants (Buseman et al., 2006; Andreou et al., 2009; Vu et al., 2012) and animals (Janssen, 2001; Wenk, 2010; Strassburg et al., 2012; Galano et al., 2017; Roy et al., 2017). Therefore, we sought to determine whether isoprostanoids could be synthesized via a nonenzymatic pathway in *P. tricornutum*, whether this synthesis could be modulated by H_2O_2, and eventually whether this class of oxylipins might have a role in stress responses.

RESULTS AND DISCUSSION

P. tricornutum Lacks Genes Coding for Enzymes Synthesizing Cyclopentane-Oxylipins

We sought to determine whether any homologs of genes coding for enzymes classically involved in the production of cyclopentane-oxylipins could be detected in the genome of *P. tricornutum*. We used, as templates, sequences from the animal kingdom (Funk, 2001) that belong to lipoxygenases (Uniprot identifier P09917), PG-endoperoxide synthases or COX2 (P35354), prostacyclin synthases (Q16647), PG-H2 D-isomerases (P41222), prostamide/PG F synthases (Q8TBF2), and PG E synthases (O14684), and sequences from the plant kingdom (Blée, 1998, 2002; Feussner and Wasternack, 2002; Andreou and Feussner, 2009) that belong to plastidial lipoxygenases (TAIR identifier AT3G45140), allene oxide synthases (AT5G42650), and allene oxide cyclases (AT3G25770). Based on BLAST searches (Altschul et al., 1990) using the Blosum62 similarity matrix and an e-value threshold of 0.1, no homologous sequence could be retrieved in the complete genomic sequences available via the Ensembl portal (http://protists.ensembl.org/Phaeodactylum_tricornutum). We could not detect any homolog of enzymes involved in the synthesis of thromboxane (e.g. Uniprot identifier P24557; Funk, 2001) or of enzymes involved in the synthesis of noncyclic oxylipins in plants (e.g. B3LF83 and Q9FPM6; Feussner and Wasternack, 2002). Therefore, *P. tricornutum* lacks the enzymatic equipment to produce cyclopentane-oxylipin and differs from other diatom species, such as *S. marinoi*, in which cyclopentane-oxylipin enzymatic pathways have been described (Gerecht et al., 2011; Gallina et al., 2016; Di Dato et al., 2017).

Detection of Isoprostanoids in *P. tricornutum* and Their Modulation upon Treatment with H_2O_2

We analyzed Pt1 (*P. tricornutum* CCMP632/CCAP 1055/1) wild-type cells incubated in the presence of increasing concentrations of H_2O_2 (0, 0.25, and 0.75 mM; Fig. 2). The total FA profile in membrane and storage glycerolipids showed moderate variations following 48 h of treatment with H_2O_2 (Fig. 2A). Consistent with past analyses (Abida et al., 2015; Popko et al., 2016), our study showed that *P. tricornutum* contains PUFA precursors for nonenzymatic oxylipins, marked by very low proportions of α-linolenic acid (18:3; less than 2% of total FAs; up to ~400 pmol per 1 million cells), ω6-arachidonic acid and ω3-eicosatetraenoic acid (20:4; less than 1%; less than 100 pmol per 1 million cells), and docosahexaenoic acid (22:6; less than 1%; less than 100 pmol per 1 million cells), and a very high content of eicosapentaenoic acid (20:5; 32%–35%; up to 10 ng per 1 million cells). After the H_2O_2 treatment, the only significant changes observed were a decrease in 16:3 and 20:5, two FAs found in galactolipids, indicating chloroplast impairment and, therefore, suggesting the amplification of ROS production following the impairment of photosynthetic capacity.

In line with previous studies (Burch and Franz, 2016), increasing doses of H_2O_2 affected *P. tricornutum* growth (Supplemental Fig. S2A) and triggered stress marked by the impairment of PSII, whose efficiency was evaluated by measuring the F_v/F_m ratio (Supplemental Fig. S2B). We observed an increased level of staining with Nile Red (Cooksey et al., 1987), a fluorescent marker of neutral lipids, only after treatment with 0.75 mM H_2O_2 (Supplemental Fig. S2C). This occurred with a significant increase in the number and size (radius = 0.423 µm, n = 71) of lipid droplets observed in *P. tricornutum* cells by epifluoresence imaging (Supplemental Fig. S2, C–E). The strong impact on chloroplasts suggests increased ROS production as a combined result of the external addition of H_2O_2 and the production of $O_2^{\bullet-}$, H_2O_2, and $OH^{\bullet}$ following organellar dysfunction.

We evaluated the presence of isoprostanoids in the same samples by using a sensitive mass spectrometry method developed recently to analyze 24 macroalgal species (Barbosa et al., 2015; Vigor et al., 2018). We sought to determine the presence of fragmentation ion products from deprotonated molecules of PhytoP, IsoP, and NeuroP in multiple reaction monitoring mode, and their detection relied on the search for previously known structures (targeted lipidomic approach). Concentrations were obtained based on calibration curves calculated using internal standards. We could detect peaks for isoprostanoids generated from all PUFAs present in *P. tricornutum*, such as PhytoP from C18:3

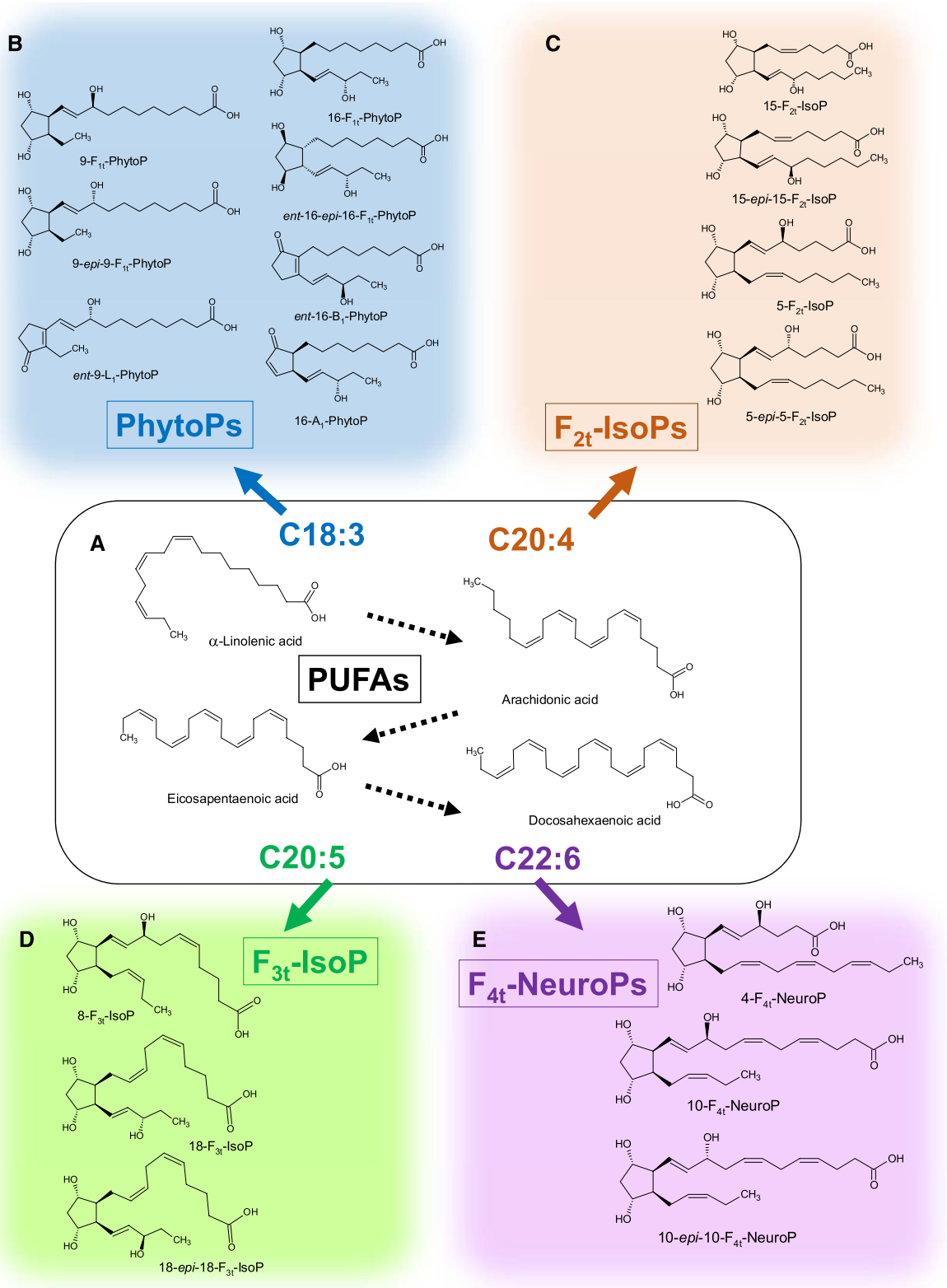

Figure 1. Chemical structures of isoprostanoids, nonenzymatic oxylipins generated from the free radical peroxidation of PUFAs. Free radicals such as $OH^{\bullet}$ trigger the peroxidation of lipids, by hydrogen abstraction from PUFAs, and the addition of molecular oxygen to form a peroxyl radical. The intermediates produced undergo a nonenzymatic series of cyclization, addition of a second molecular oxygen, and reduction to form prostanoids. A, Main PUFAs. B, PhytoPs from α-linolenic acid. C, F_{2t}-IsoPs from arachidonic acid. D, F_{3t}-IsoPs from eicosapentaenoic acid. E, F_{4t}-NeuroPs from docosahexaenoic acid. A large number of isoprostanoids can be formed from each PUFA substrate. The scheme shows the main structures analyzed in this study.

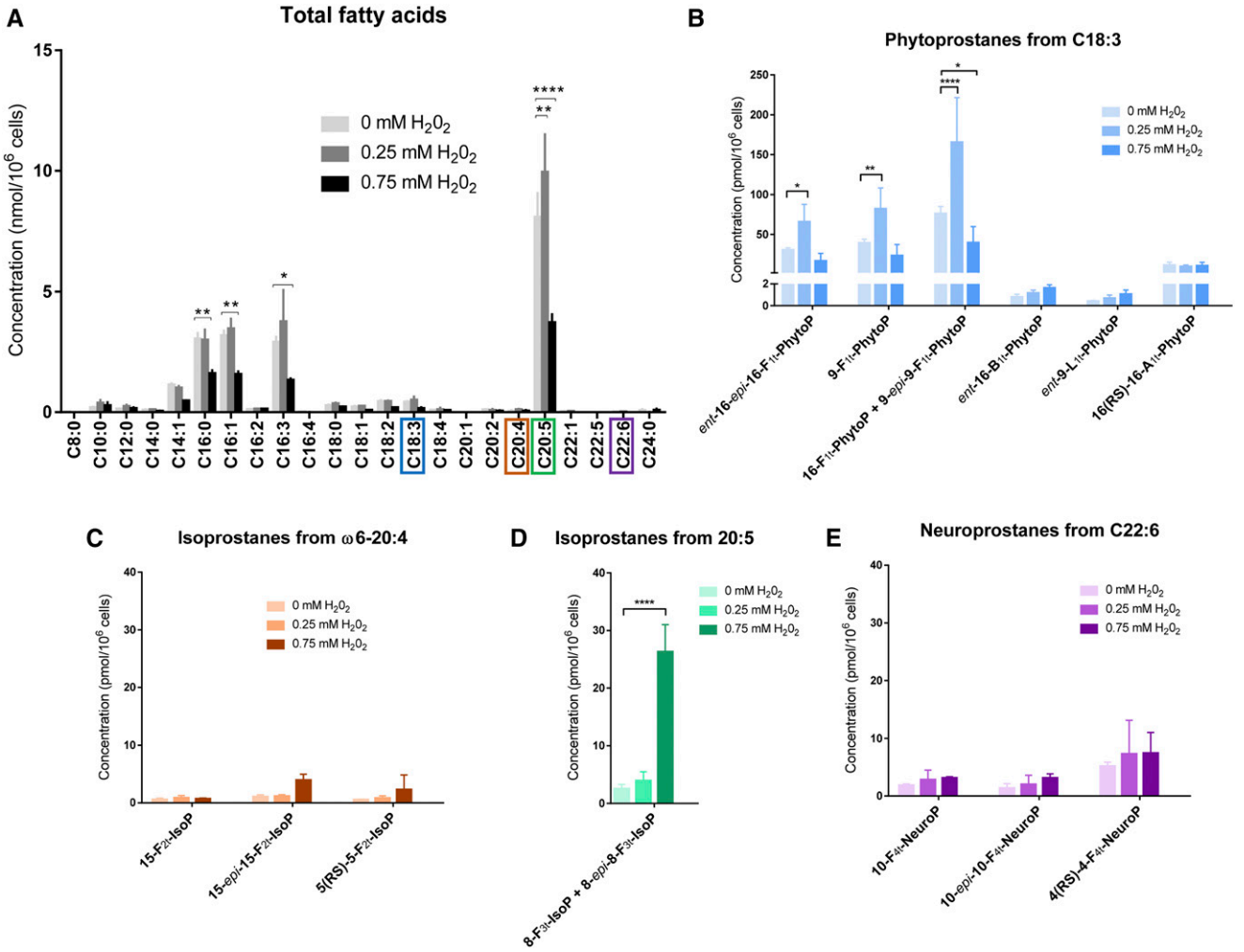

Figure 2. Characterization of PhytoPs, NeuroPs, and IsoPs in *P. tricornutum* cells. The incubation was performed in a volume of 50 mL, inoculated at 5×10^6 cells mL^{-1}. Lipids were extracted and analyzed after 48 h of incubation in the presence of H_2O_2 at the indicated doses. A, Total FA profile for increasing doses of H_2O_2. B, Concentration of phytoprostanes from α-linolenic acid normalized with the cell concentration. C18:3 and corresponding phytoprostanes are shown in blue. C and D, Concentrations of F_{2t}-IsoPs and F_{3t}-IsoPs from eicosatetraenoic and eicosapentaenoic acids. C20:4 and C20:5 and corresponding isoprostanes are shown in brown and green, respectively. E, Concentration of F_{4t}-NeuroPs from docosahexaenoic acid. C22:6 and corresponding neuroprostane are shown in purple. Values correspond to three biological replicates. Statistically relevant responses (two-way ANOVA with Dunnett's posthoc test) are indicated by asterisks: *, $P < 5 \times 10^{-2}$; **, $P < 5 \times 10^{-3}$; and ****, $P < 10^{-4}$.

(*ent*-16-*epi*-16-F_{1t}-PhytoP, 9-F_{1t}-PhytoP, *ent*-16-B_{1t}-PhytoP, *ent*-9-L_{1t}-PhytoP, and peaks corresponding to either 16-F_{1t}-PhytoP or 9-*epi*-9-F_{1t}-PhytoP; Fig. 2B), IsoP from C20:4 (15-F_{2t}-IsoP, 15-*epi*-15-F_{2t}-IsoP, and 5(*R*/*S*)-5-F_{2t}-IsoP; Fig. 2C), IsoP from C20:5 (peaks corresponding to either 8-F_{3t}-IsoP or 8-*epi*-8-F_{3t}-IsoP; Fig. 2D), and NeuroP from C22:6 (4(*RS*)-4-F_{4t}-NeuroP, 10F_{4t}-NeuroP, and 10-*epi*-10-F_{4t}-NeuroP; Fig. 2E).

Based on these targeted analyses, although C18:3 represents a minor FA substrate, PhytoPs constitute the main family of nonenzymatic oxylipins in *P. tricornutum* (up to 300 pmol of total PhytoP per 1 million cells), in the same concentration range as that of nonoxidized C18:3 (up to 400 pmol per 1 million cells). The F_{1t}-PhytoP series is the most abundant, as recorded previously in C18:3-rich plant species (Collado-González et al., 2015) and in all studies on Chlorophyta, Phaeophyta, and Rhodophyta macroalgae so far (Barbosa et al., 2015). In plants, F_{1t}-PhytoPs are in the same concentration range as phytooxylipins of the enzymatic pathway, such as 12-oxo-phytodienoic acid or jasmonic acid (Parchmann and Mueller, 1998; Imbusch and Mueller, 2000; Thoma et al., 2003). The low concentrations of *ent*-16-B_{1t}-PhytoP as well as the very low level of 16(*RS*)-16-A_{1t}-PhytoPs indicate that radical peroxidation of α-linolenic acid preferentially activates the pathway of F_{1t}-PhytoP. Interestingly, we did not detect any D_1- and J_1-PhytoP in the cultures of *P. tricornutum* cells, two series of phytoprostanes commonly found in higher plants (Jahn et al., 2010; Collado-González et al., 2015).

A significant increase in the F_{1t}-PhytoP concentration occurred after treatment with 0.25 mM H_2O_2 ($P = 0.0163$ for *ent*-16-*epi*-16-F_{1t}-PhytoP, $P = 0.0012$ for 9-F_{1t}-PhytoP, and $P < 0.0001$ for compounds with fragmentation peaks corresponding to those of 16-F_{1t}-PhytoP and/or 9-*epi*-9-F_{1t}-PhytoP), whereas a wild-type concentration level was observed after a nearly lethal treatment with 0.75 mM H_2O_2. Concentrations of A_{1t}-, B_{1t}-, and L_{1t}-PhytoPs remained very low and appeared unaffected by the treatment (less than 1 ng per 1 million cells; Fig. 2B). H_2O_2 is known to further oxidize isoprostanoids into toxic aldehydes (Long et al., 2008). We do not exclude the possibility that PhytoPs might be further oxidized under very strong oxidative stress conditions.

In *P. tricornutum*, only a minor portion of C20:4 corresponds to *ω*6-arachidonic acid (*ω*6-C20:4), the main being eicosatetraenoic acid (*ω*3-C20:4; Arao et al., 1987, 1994; Arao and Yamada, 1994; Abida et al., 2015; Dolch and Maréchal, 2015). Nevertheless, three isoprostanes of the F_{2t} series (15-F_{2t}-IsoP, 15-*epi*-15-F_{2t}-IsoP, and 5(*RS*)-5-F_{2t}-IsoP) derived from *ω*6-C20:4 could be detected (Fig. 2C). These F_{2t}-IsoPs remained in very low concentrations and did not accumulate in high levels upon H_2O_2 treatment.

Surprisingly, although C20:5 is the most abundant FA in unstressed *P. tricornutum* cells (~300 ng per 1 million cells; Fig. 2A), due to its very high level in some classes of membrane lipids (Abida et al., 2015; Dolch and Maréchal, 2015), only a low concentration of 8(*RS*)-8-F_{3t}-IsoP could be detected (~2–30 pmol per 1 million cells; Fig. 2D). As observed for IsoPs derived from C20:4, the concentration of 8(*RS*)-8-F_{3t}-IsoP increased as a function of H_2O_2 ($P < 0.0001$).

Although C22:6 is a very minor FA in *P. tricornutum*, we detected three neuroprostanes, 10-F_{4t}-NeuroP, 10-*epi*-10-F_{4t}-NeuroP, and 4(*RS*)-4-F_{4t}-NeuroP, in the same concentration range as nonoxidized C22:6 (Fig. 2E). No significant difference was observed in NeuroP concentrations after treatment with higher doses of H_2O_2.

PC and/or DGTA Are Potential Precursors for Nonenzymatic Production of Isoprostanoids

By contrast with enzymatically produced prostanoids, isoprostanoids are generated on esterified lipids prior to their release as free oxidized lipids by phospholipases A_2 (Morrow et al., 1992; Ibrahim et al., 2011a). Phytoprostanes of the F1 series being the most abundant in *P. tricornutum*, we sought to determine which lipid class could represent a likely source of the corresponding C18:3 substrate, both in unstressed conditions and upon treatment with H_2O_2 (Fig. 3).

The complete profile of glycerolipids showed a significant decrease in MGDG and an increase in TAG at 0.75 mM H_2O_2 (Fig. 3A). In striking contrast to other stress conditions, which trigger the accumulation of TAGs enriched in C16:0 and C16:1 (Abida et al., 2015), treatment with H_2O_2 triggered the accumulation of TAG molecular species enriched in PUFAs and VLC-PUFAs (Fig. 3B). This indicates a synthesis from recycled C16:2-, C16:3-, and C20:5-rich membrane lipids rather than de novo synthesis from C16:0- and C16:1-rich diacyl precursors. Such diversion of PUFAs to TAG has been reported previously in *Drosophila melanogaster* stem cells exposed to oxidative damage, including H_2O_2 treatment, and interpreted to be a mechanism to protect PUFAs from excessive and harmful peroxidation (Bailey et al., 2015). The presence of C16:3 in TAG reflects the incorporation of acyl moieties derived from chloroplast lipids that contain this FA in high proportions, possibly from MGDG and, to a lower extent, DGDG (Fig. 3C). An MGDG-to-TAG conversion is supported further by the decrease in C16:3- and C20:5-rich MGDG molecular species. The concentration of another chloroplast lipid, SQDG, also declines (Fig. 3C), with little modifications in its molecular species. By contrast, the PG level decreases significantly at high H_2O_2 concentration, mainly due to a decrease in C16:0/C16:1 and C16:1/C16:1 molecular species, possibly reflecting the impact on one of the PG pools in *P. tricornutum* cells (i.e. in the chloroplast, the mitochondrion, or the endoplasmic reticulum). Since no subcellular lipidome has been identified to date for any of these compartments in diatoms, the identity of the pool of PG affected by H_2O_2 could not be characterized further.

It is interesting that the global DGDG level is unaffected by H_2O_2 treatment (Fig. 3A). Nevertheless, the FA profile of DGDG is modified, showing an increase in the level of molecular species such as C20:5/C16:0, C20:5/C16:2, and C20:5/C16:3, some of which could be derived from MGDG. In addition to an MGDG-to-TAG conversion, the MGDG-to-DGDG pathway likely is activated.

Galactolipids contain high levels of C20:5 (Fig. 3C). The ratio of F_{3t}-IsoP/unoxidized C20:5 being lower than 1% to 10%, it is possible that galactolipids are not an important platform for F_{3t}-IsoP production. Such a low proportion of isoprostanoids has been reported earlier in a comprehensive analysis of oxylipins esterified to plant galactolipids (Ibrahim et al., 2011b).

Only PC and DGTA contained sufficient amounts of C18:3 to justify a role as a substrate glycerolipid for the production of PhytoP (taking into account that 2 nmol of FA corresponds to 1 nmol of glycerolipid; Fig. 3C). In addition, these two glycerolipid classes also contain C20:4, C20:5, and C22:6 acyl groups, which could be involved in the production of other IsoPs and NeuroPs detected in *P. tricornutum*. Therefore, one or both of these lipids might be the platform for the nonenzymatic production of prostanoids in *P. tricornutum*. Given the fact that the ratio of total PhytoP to nonoxidized C18:3 is close to 1 and that of NeuroP to nonoxidized C22:6 is higher than 1, one would expect the production of isoprostanoids from PC and DGTA to be intense and to have a biological function.

Dose-Response Effect of Isoprostanoids on *P. tricornutum*

Isoprostanoids have been considered indicators of oxidative stress for decades. The study of their biological

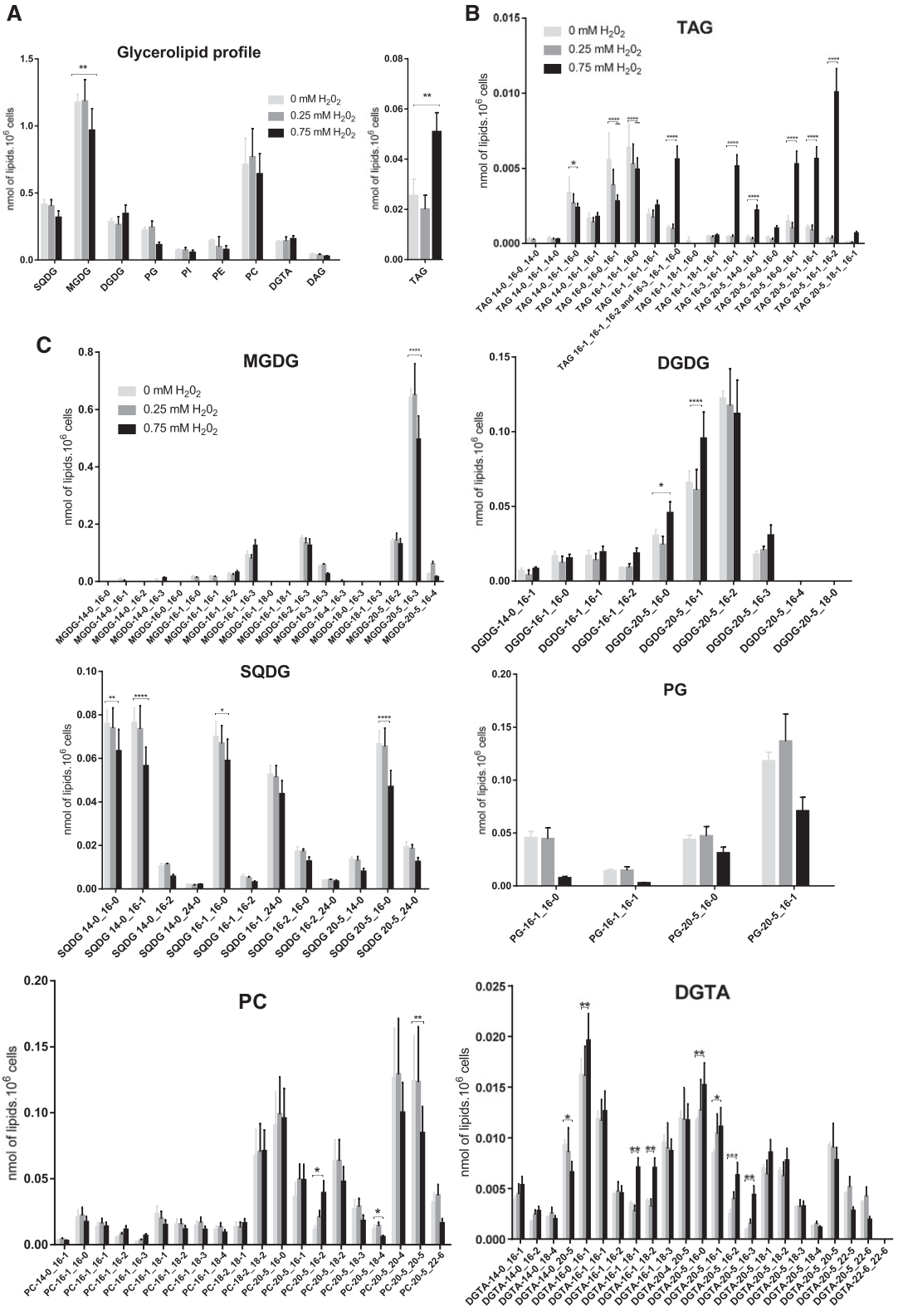

Figure 3. Glycerolipid profile following treatment with H_2O_2. *P. tricornutum* cells were cultivated in Enriched Seawater, Artificial Water medium using 10 times enriched nitrogen and phosphate sources (ESAW 10N10P) until a cell density of 5×10^6 cells mL^{-1} was reached. Cells then were incubated for 48 h in the presence or absence of H_2O_2, as indicated. Lipids were extracted and analyzed as described in "Materials and Methods." A, Glycerolipid profile following treatments with increasing doses of H_2O_2. Glycerolipid concentrations are expressed in nmol per 1 million cells. B, Fatty acid profile of TAG. C, Fatty acid

action is still in its infancy, particularly in photosynthetic organisms. Evidence on specific functions that could be attributed to isoprostanoids was sought initially in animal models. Thus, IsoPs were shown to act as agonists or antagonists binding to prostanoid receptors, among them the thromboxane receptor, PG F2 receptor, PG E2 subtype 3 receptor, and PG D2 subtype 2 receptor (Janssen, 2001; Milne et al., 2011; Galano et al., 2017). Recently, drugs acting on prostanoid receptors were identified in a pharmacological screen, which screened for the accumulation of lipid droplets in *P. tricornutum* cells (Conte et al., 2018), suggesting that prostanoid/isoprostanoid-sensing systems also could be present and control TAG biosynthesis in diatoms.

Therefore, we investigated if some of the compounds identified here could have a similar impact on *P. tricornutum* phenotype. To that purpose, we analyzed *P. tricornutum* cell culture incubated in the presence of nine synthetic isoprostanoids added at concentrations in the micromolar range (i.e. at 0, 5, 25, and 50 μM; Fig. 4). For PhytoP, we tested the B_1 and L_1 series and their diastereoisomers (Fig. 4, A–D), which are minor compounds in the *P. tricornutum* cultures (Fig. 2B). We analyzed the effects of four F_{3t}-IsoPs, which could be derived from the peroxidation of C20:5 (Fig. 4, E–H). Eventually, we tested the NeuroP detected in *P. tricornutum* cells (i.e. 4(*RS*)-4-F_{4t}-NeuroP, derived from the peroxidation of C22:6; Figs. 2D and 4I). We observed similar effects for all isoprostanoids, most strikingly a 10% to 20% decrease in the cell concentration at the lowest doses (5 μM), with the exception of 9-L_1-PhytoPs, with growth being affected at 25 μM (Fig. 4). An impact on cell division has been reported previously in Arabidopsis (*Arabidopsis thaliana*), in which a treatment with 25 μM A_1-PhytoP reduced the growth of roots by almost half (Mueller et al., 2008). This impact on growth also was noticed in mutant plants that lack tocopherols, which results in a lack of control of nonenzymatic lipid peroxidation during early development (Sattler et al., 2006).

Staining with Nile Red showed a 10% to 30% increase in the levels of the four PhytoPs at 50 μM at 48 h after incubation; this supports the induction of neutral lipid accumulation (Fig. 4, A–D). An increase in Nile Red staining also was observed at low doses of IsoP and NeuroP (5 μM), and the levels returned to the control level at higher concentrations (50 μM; Fig. 4, E–I). The activity of PSII as assessed by the F_v/F_m ratio was stable in cultures incubated with any of the tested isoprostanoids regardless of the concentration (Fig. 4).

Isoprostanoids, therefore, seem to trigger some of the effects observed after H_2O_2 treatment, in particular, a decrease in growth and an increase in the levels of neutral lipids; however, no deleterious impact of H_2O_2 on photosynthesis was observed. Assuming an average cell volume of 65 μm^3 (Li et al., 2012) for *P. tricornutum*, the consolidated cell volume in 1×10^6 cells can be calculated to be 65 μL. The bioactive concentrations of isoprostanoids (i.e. triggering an effect on *P. tricornutum*) ranged from 10 to 300 pmol per 1 million cells (Fig. 2; i.e. in the 0.15 to 4 μM range). Are these concentrations consistent with a role in cell-to-cell communication (i.e. as molecules known as infochemicals) or a role as intracellular mediators? In the oceanic environment, the expected concentrations for a possible role as a cell-to-cell mediator is in the low picomole to nanomole range, which is far below the concentrations found in this study to speculate on isoprostanoids serving as infochemicals. Rather, the dose-response analyses we performed, which showed a biological effect on *P. tricornutum* cells (Fig. 4), represent realistic conditions for intracellular mediators. Thus, we propose a model for the induction of isoprostanoids in *P. tricornutum* and their activity (Fig. 5). First, this model considers environmental conditions that induce stress in diatoms, leading directly or indirectly to the dysfunction of organelles like the chloroplast, the mitochondrion, or the peroxisome or triggering an oxidative burst, such as that occurring in some biotic interactions in plants. Such series of cellular effects occur in the majority of abiotic and biotic stresses. ROS are then produced, including $O_2^{\bullet-}$, H_2O_2, and, following the different reactions described above, $OH^{\bullet}$. If protective systems fail to control the oxidative stress, lipid peroxidation can occur, essentially at the level of PC and/or DGTA, containing the sufficient amounts of FA substrates to allow the generation of PhytoP, IsoP, and NeuroP. These isoprostanoids inhibit growth and induce the production of TAG via an unknown process. It is possible that isoprostanoids regulate the MGDG-to-TAG conversion and, thus, contribute to this PUFA protection mechanism. Isoprostanoids apparently have no effect on photosystems, indicating that another mechanism is involved to account for the susceptibility of PSII to H_2O_2. Other biological actions might be controlled by isoprostanoid signaling, possibly at the transcriptional level. In plants, PhytoPs were shown to regulate gene expression (Thoma et al., 2003; Loeffler et al., 2005; Mueller et al., 2008), up-regulating genes related to detoxification, stress response, and pathways not associated with chloroplasts and photosynthesis.

CONCLUSION

The production of oxidized FAs in *P. tricornutum* has remained unexplained for decades. No gene equipment seems present to allow the production of canonical prostanoids, such as jasmonic acids or prostaglandins

Figure 3. (*Continued*.)
profiles of membrane glycerolipids following treatment with increasing doses of H_2O_2. Data correspond to biological triplicates ± SD. SQDG, Sulfoquinovosyldiacylglycerol. Values correspond to three biological replicates. Statistically relevant responses (two-way ANOVA with Dunnett's posthoc test) are indicated by asterisks: *, $P < 5 \times 10^{-2}$; **, $P < 5 \times 10^{-3}$; and ****, $P < 10^{-4}$.

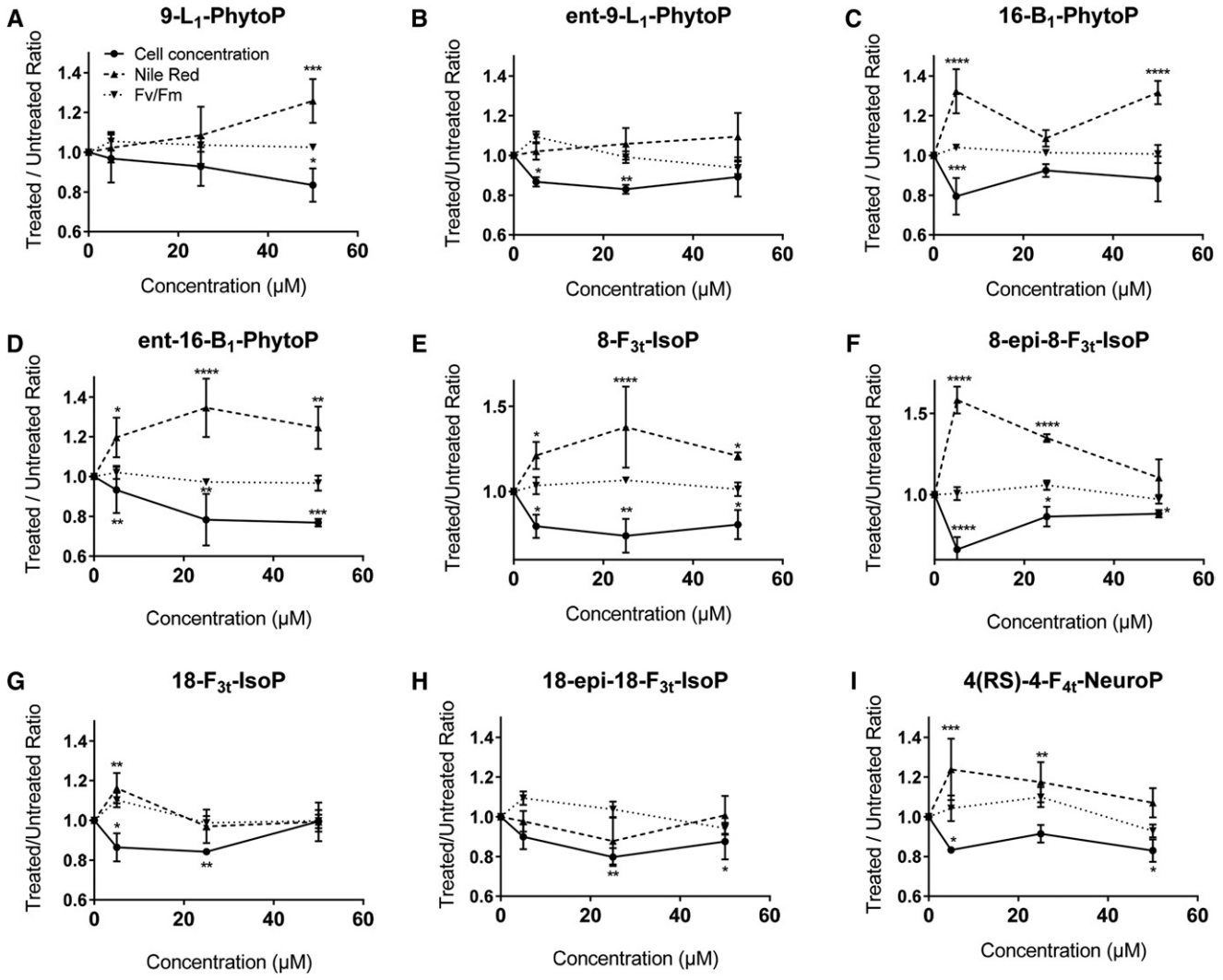

Figure 4. Effects of PhytoPs, IsoPs, and NeuroPs on *P. tricornutum* cells. Values correspond to three biological replicates. A 48-h incubation was performed in a volume of 2 mL, on 24-well plates, inoculated at 10^6 cells mL^{-1}, with immediate addition of chemicals. Three concentrations of each isoprostanoid were tested (5, 25, and 50 μM). Incubations were performed with 9-L_1-PhytoP (A), *ent*-9-L_1-PhytoP (B), 16-B_1-PhytoP (C), *ent*-16-B_1-PhytoP (D), 8-F_{3t}-IsoP (E), 8-*epi*-8-F_{3t}-IsoP (F), $^{18}F_{3t}$-IsoP (G), 18-*epi*-$^{18}F_{3t}$-IsoP (H), and 4(*RS*)-4-F_{4t}-NeuroP (I). Cell growth (circles), Nile Red accumulation (squares), and the PSII quantum efficiency F_v/F_m (triangles) were measured after 48 h of treatment as described in "Materials and Methods." Results were normalized to untreated controls. Statistically relevant responses (two-way ANOVA) are indicated by asterisks: *, $P < 5 \times 10^{-2}$; **, $P < 5 \times 10^{-3}$; ***, $P < 1.1^{-3}$; and ***, $P < 1.1^{-4}$.

and thromboxanes. This phenomenon is not specific to all diatoms, since other species, such as *S. marinoi*, have oxylipin biosynthetic pathways producing prostanoids (Gerecht et al., 2011; Gallina et al., 2016; Di Dato et al., 2017). A first line of investigation focused on the possible production of polyunsaturated aldehydes (PUAs). After wounding or exposure to nutrient stresses, diatom PUFAs were shown to be oxidized enzymatically into volatile PUAs, including 2*E*,4*E*-decadienal (Miralto et al., 1999). PUAs initially were considered potent interspecific and intraspecific signaling compounds, triggering programmed cell death (Casotti et al., 2005; Vardi et al., 2006) and possibly acting as infochemicals in population size control. However, PUAs could not be detected in *P. tricornutum* lipidomic analyses (Collins et al., 2016); therefore, they might be present at extremely low levels. Effects of PUAs on *P. tricornutum* were detected in the high 20 μM range, which seems above the concentration expected for a cell-to-cell mediation by multiple orders of magnitude, making PUAs unlikely infochemicals. The mode of action of PUAs via the activation of nitric oxide was reevaluated recently (Dolch et al., 2017). That study characterizes nonenzymatic cyclopentane-oxylipins in *P. tricornutum*, in high intracellular concentrations, which is consistent with their function as signaling compounds. Not

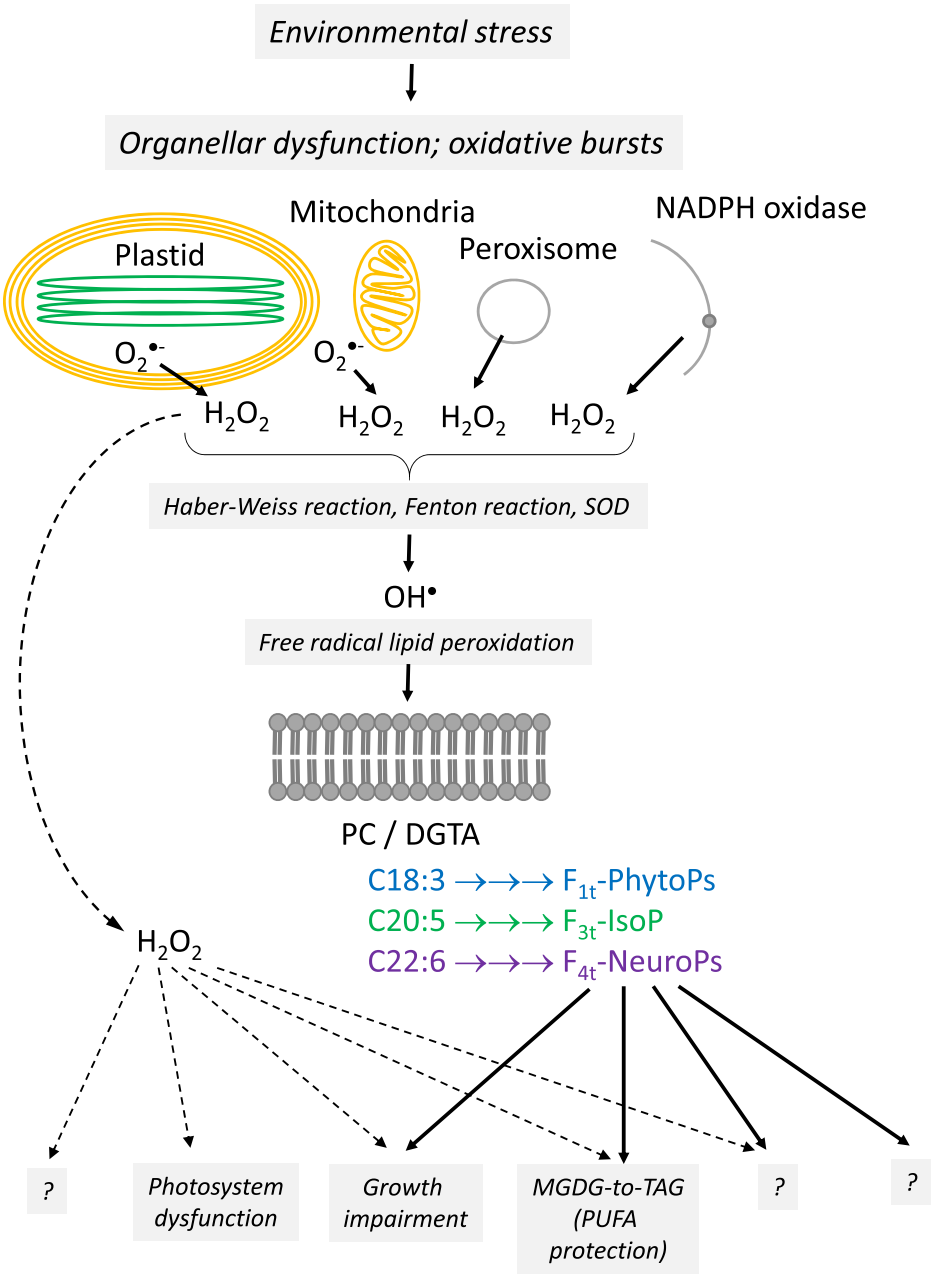

Figure 5. Model for nonenzymatic isoprostanoid production and a specific role in ROS-dependent signaling pathways in *P. tricornutum*.

all membrane lipids seem to be appropriate for their production, since only PC and DGTA have the most coherent FA profile with the molecular diversity of isoprostanoids produced. F_{1t}-PhytoP produced from C18:3 is the most abundant form. The production of NeuroP also can explain why a very low basal level of C22:6 is maintained in PC and DGTA, whereas other glycerolipids seem to contain only traces of this FA or to not contain any. We provide evidence that isoprostanoids are potential intracellular mediators, partly responsible for TAG accumulation triggered by oxidative stress.

The high content of PUFAs and VLC-PUFAs inside these lipid droplets suggests a role in the protection of FAs sensitive to oxidation. A similar mechanism might control the accumulation of small lipid droplets in *P. tricornutum* exposed to nitric oxide, as $NO^{\bullet}$ is known to react with $O_2^{\bullet-}$ to form $ONOO^-$ ions, which is involved in the nitrosylation and peroxidation of lipids (Janssen, 2001). Excessive oxidative conditions can lead to the conversion of isoprostanoids into toxic aldehydes (Long et al., 2008), as one of the entry points toward necrosis. Potential foci for future research include the exploration of environmental conditions

triggering isoprostanoid production in *P. tricornutum* and the identification of molecular and cell components involved in their control. Large-scale cultures treated with synthetic isoprostanoids should allow refined analyses of transcriptomic, proteomic, and lipidomic changes that will help characterize the components of the signaling pathways. Finally, microalgal oil is considered a promising resource for the development of biofuels and green chemistry; therefore, it is relevant to identify the molecular mechanisms driving the accumulation of unsaturated FA/monounsaturated FA inside TAGs in conditions such as nutrient stress and those involved in the protection of PUFAs inside TAGs under oxidative stress and the likely combination of both under numerous conditions.

MATERIALS AND METHODS

Chemicals

The chemicals used in the composition of growth media and 30% (v/v) H_2O_2 were obtained from Sigma-Aldrich. Eight PhytoP standards (9-L$_1$-PhytoP, *ent*-9-L$_1$-PhytoP, *ent*-16-*epi*-16-F$_{1t}$-PhytoP, 9F$_{1t}$-PhytoP, 16F$_{1t}$-PhytoP + 9-*epi*-9-F$_{1t}$-PhytoP, 16(*RS*)-16-A$_{1t}$-PhytoP, 16-B$_1$-PhytoP, and *ent*-16-B$_1$-PhytoP), three NeuroP standards (4(*RS*)-4-F$_{4t}$-NeuroP, 10-F$_{4t}$-NeuroP, and 10-*epi*-10-F$_{4t}$-NeuroP), and eight IsoP standards (8-F$_{3t}$-IsoP, 8-*epi*-8-F$_{3t}$-IsoP, ^{18}F$_{3t}$-IsoP, 18-*epi*-^{18}F$_{3t}$-IsoP, 15-F$_{2t}$-IsoP, 15-*epi*-15-F$_{2t}$-IsoP, 5-F$_{2t}$-IsoP, and 5-*epi*-5-F$_{2t}$-IsoP) were chemically synthesized (Durand et al., 2004; El Fangour et al., 2005; Oger et al., 2010; Guy et al., 2014, 2015). The internal standard d$_4$-15-F$_{2t}$-IsoP was acquired from Cayman Chemicals.

Cultivation of *Phaeodactylum tricornutum*

P. tricornutum (Pt1) Bohlin Strain 8.6 CCMP2561 (Culture Collection of Marine Phytoplankton, now known as NCMA: National Center for Marine Algae and Microbiota) was used in all experiments. Pt1 cells were maintained and grown in a volume of 50 mL in 100-mL flasks or in a volume of 2 mL on 24-well plates at 20°C in a modified ESAW medium (NaCl 362.7 mM, Na_2SO_4 25 mM, KCl 8.03 mM, $NaHCO_3$ 2.067 mM, KBr 0.725 mM, H_3BO_3 0.372 mM, NaF 0.0657 mM, $MgCl_2$ 47.18 mM, $CaCl_2$ 9.134 mM, $SrCl_2$ 0.082 mM, Na_2-glycerophosphate 21.8 µM, Na_2SiO_3 105.6 µM, Na_2EDTA 14.86 µM, $Fe(NH_4)_2(SO_4)_2$ 5.97 µM, $FeCl_3$ 0.592 µM, $MnSO_4$ 2.42 µM, $ZnSO_4$ 0.254 µM, $CoSO_4$ 0.0569 µM, Na_2MoO_4 0.52 µM, H_3BO_3 61.46 µM, Na_2SeO_3 10 nM, biotin [vitamin H] 8.18 nM, cobalamin [vitamin B_{12}] 2.94 nM, and thiamine [vitamin B_1] 0.594 µM; Falciatore et al., 2000) using ESAW 10N10P, containing 5.49 mM $NaNO_3$ and 0.224 mM NaH_2PO_4; Abida et al., 2015). Cells were grown on a 12/12-h light (50 µE m^{-2} s^{-1})/dark cycle. Growth was evaluated by cell counting using a TECAN Infinite M1000Pro plate reader and determined following the equation $y = 1.834 \times 10^{-08}$ $x + 0.03758$, where x = the A_{730} and y = the number of cells (Conte et al., 2018).

Incubation of *P. tricornutum* with H_2O_2

From a stock solution of 9.79 M H_2O_2 (Sigma-Aldrich), a 0.5 M stock solution was prepared freshly and dissolved in ESAW 10N10P medium. A 50-mL volume of *P. tricornutum* was incubated at a cell density of 5×10^6 cells mL^{-1}, in 100-mL flasks, with different concentrations of H_2O_2 (0, 0.25, and 0.75 mM) during 48 h. These H_2O_2 concentrations were defined empirically based on *P. tricornutum* growth. Incubations were performed in independent biological triplicates. Growth was quantified based on absorption at 730 nm using a TECAN Infinite M1000Pro plate reader and normalized with the untreated control (Conte et al., 2018).

Incubation of *P. tricornutum* with PhytoPs, NeuroPs, and IsoPs

A 2-mL volume of a *P. tricornutum* culture was inoculated at a cell density of 10^6 cells mL^{-1}, on 24-well plates, and incubated with different concentrations of isoprostanoids (0, 5, 25, and 50 µM) solubilized in methanol (final concentration, 1%) during 48 h. Growth was quantified based on absorption at 730 nm using a TECAN Infinite M1000Pro plate reader and normalized with the untreated control (Conte et al., 2018).

Chlorophyll Fluorescence and Photosynthetic Parameters

To determine photosynthesis parameters in cell cultures, room temperature fast chlorophyll fluorescence kinetics was measured using a Speedzen MX fluorescence imaging system (JBeamBio) with previously described settings (Johnson et al., 2009; Allorent et al., 2013). To this end, a 150-µL volume of *P. tricornutum* culture was transferred to a transparent 96-well plate and dark incubated for 15 to 30 min before measurements. Excitation was performed in the blue range (λ = 450 nm; F_0). F_0 is the steady-state fluorescence in dark-adapted cultures, and F_m is the maximal fluorescence after a saturating light pulse with green light (520 nm) of dark-adapted cultures. F_v is the difference between F_m and F_0. With these parameters, the maximum efficiency of energy conversion of PSII can be calculated as F_v/F_m (Butler and Kitajima, 1975; Misra et al., 2012).

Imaging of TAG Accumulation in *P. tricornutum* Cells Based on Nile Red Staining

The accumulation of TAG droplets in lipid droplets in the cytosol was monitored using Nile Red (Sigma-Aldrich) fluorescent staining (excitation wavelength at 485 nm, emission at 525 nm) as described previously (Cooksey et al., 1987; Abida et al., 2015; Conte et al., 2018). In brief, cells were diluted and adjusted to a cell density that was linearly correlated with Nile Red fluorescence. Nile Red solution (40 µL of a 2.5 µg mL^{-1} stock solution in dimethyl sulfoxide) was added to 160-µL cell suspensions. Nile Red fluorescence values were normalized to the cell concentration. Lipid droplets stained with Nile Red were then visualized using a Zeiss LSM800 confocal laser scanning microscope equipped with a Zeiss Plan-APO 63× numerical aperture, 1.46 oil-immersion objective and enlarged 4×. Nile Red fluorescence was monitored by excitation at 488 nm and a capture zone ranging from 579 to 641 nm. Chlorophyll autofluorescence was monitored by excitation at 488 nm and a capture zone ranging from 650 to 700 nm. Bright-field acquisition was performed in parallel. Acquired images were imported and analyzed with ImageJ 1.48v using the BIO-FORMATS plugins 5.7.2. Student's *t* test was performed to compare the means of lipid droplet dimensions (radius).

Glycerolipid Extraction and Profiling

Glycerolipids were extracted from freeze-dried *P. tricornutum* cells grown in 50 mL of ESAW medium. About 50×10^6 to 100×10^6 cells are required for a triplicate analysis. First, cells were harvested by centrifugation and immediately frozen in liquid nitrogen. Once freeze dried, the pellet was suspended in 4 mL of boiling ethanol for 5 min to prevent lipid degradation, and lipids were extracted as described previously (Simionato et al., 2013) by the addition of 2 mL of methanol and 8 mL of chloroform at room temperature. The mixture was then saturated with argon and stirred for 1 h at room temperature. After filtration through glass wool, cell debris was rinsed with 3 mL of chloroform:methanol (2:1, v/v), and 5 mL of 1% NaCl was then added to the filtrate to initiate phase separation. The chloroform phase was dried under argon before solubilizing the lipid extract in 1 mL of chloroform. Total glycerolipids were quantified from their FAs: in a 10-µL aliquot fraction, a known quantity of saturated 15-carbon FA (15:0) was added and all FAs were methanolyzed into methyl esters (FAMEs) by a 1-h incubation in 3 mL of 2.5% H_2SO_4 in pure methanol at 100°C (Jouhet et al., 2003). The reaction was stopped by the addition of 3 mL of water, and 3 mL of hexane was added for phase separation. After 20 min of incubation, the hexane phase was transferred to a new tube. FAMEs were extracted a second time via the addition, incubation, and extraction of another 3 mL of hexane. The combined collected hexane fractions (6 mL) were argon dried, and FAMEs were suspended in 40 µL of hexane for analysis by gas chromatography coupled with flame ionization detection (Perkin-Elmer), using a BPX70 (SGE) column. FAMEs were identified by comparison of their retention times with those of standards (Sigma-Aldrich) and quantified by the surface peak method using 15:0 for calibration.

Extraction and quantification were performed with three biological replicates. Glycerolipids were then analyzed and quantified by HPLC-tandem mass spectrometry, with appropriate standard lipids (Jouhet et al., 2017). In brief, lipid extracts corresponding to 25 nmol of total FAs were dissolved in 100 µL of chloroform:methanol (2:1, v/v) containing 125 pmol of each internal

standard. The internal standards used were phosphatidylethanolamine 18:0-18:0 and diacylglycerol 18:0-22:6 from Avanti Polar Lipids and SQDG 16:0-18:0 extracted from spinach (*Spinacia oleracea*) thylakoid (Demé et al., 2014) and hydrogenated (Buseman et al., 2006). Lipids then were separated by HPLC and quantified by tandem mass spectrometry. Lipid classes were separated using an Agilent 1200 HPLC system using a 150-mm × 3-mm (length × i.d.) 5-µm diol column (Macherey-Nagel) at 40°C. The mobile phases consisted of hexane:isopropanol:water:1 M ammonium acetate, pH 5.3 (625:350:24:1, v/v/v/v; A), and isopropanol:water:1 M ammonium acetate, pH 5.3 (850:149:1, v/v/v; B). The injection volume was 20 µL. After 5 min, the percentage of B was increased linearly from 0% to 100% in 30 min and kept at 100% for 15 min. This elution sequence was followed by a return to 100% A in 5 min and an equilibration for 20 min with 100% A before the next injection, leading to a total run time of 70 min. The flow rate of the mobile phase was 200 µL min^{-1}. The distinct glycerophospholipid classes were eluted successively as a function of the polar head group.

Mass spectrometric analysis was performed on a 6460 triple quadrupole mass spectrometer (Agilent) equipped with a jet stream electrospray ion source under the following settings: drying gas heater at 260°C, drying gas flow at 13 L min^{-1}, sheath gas heater at 300°C, sheath gas flow at 11 L min^{-1}, nebulizer pressure at 25 p.s.i., capillary voltage at ±5,000 V, and nozzle voltage at ±1,000 V. Nitrogen was used as the collision gas. PC and DGTA analyses were carried out in positive ion mode by scanning for precursors of mass-to-charge ratio 184 and 236, respectively, at collision energy (CE) of 34 and 52 eV. SQDG analysis was carried out in negative ion mode by scanning for precursors of mass-to-charge ratio −225 at CE of −56 eV. Phosphatidylethanolamine, phosphatidylinositol, PG, MGDG, and DGDG measurements were performed in positive ion mode by scanning for neutral losses of 141, 277, 189, 179, and 341 D at CEs of 20, 12, 16, 8, and 8 eV, respectively. Diacylglycerol and TAG species were identified and quantified by multiple reaction monitoring as singly charged ions $[M+NH_4]^+$ at CE of 16 and 22 eV, respectively. Each lipid species was quantified by multiple reaction monitoring with a 50-ms dwell time and the various transitions recorded previously (Abida et al., 2015). Mass spectra were processed using the MassHunter Workstation software (Agilent) for the identification and quantification of lipids. Lipid amounts (pmol) were corrected for response differences between internal standards and endogenous lipids and by comparison with a qualified control. Qualified control extracts correspond to a known *P. tricornutum* lipid extract qualified previously and quantified by thin-layer chromatography and gas chromatography coupled to flame ionization detection, as described earlier (Jouhet et al., 2017).

Isoprostanoid Extraction and Mass Spectrometry Analyses

Samples (30 mg dry weight) of *P. tricornutum* cells were ground for 30 s into 1 mL of 0.025% (w/v) butylated hydroxytoluene in methanol, using a FastPrep-24 (MP Biomedicals) homogenizer set at maximum velocity (6.5 m s^{-1}). Samples were then transferred to clean vials, to which were added 1 mL of MeOH, 1.5 mL of phosphate buffer (pH 2), and 6 µL of isoprostanoid internal standard mix. This mixture was stirred for 1 h at 100 rpm (1.7*g*) at room temperature. Then, samples were centrifuged at 3,000*g* for 5 min. The supernatant was recovered, and 4 mL of cold chloroform was added. Samples were then stirred for 30 s and centrifuged at 3,000*g* for 5 min at room temperature. The chloroform phase was separated and concentrated under nitrogen (0.7 bar) at 40°C during 1 h. Hydrolysis then was performed with 950 µL of 1 M KOH mixed during 30 min at 40°C. At the end, 1 mL of 0.04 M formic acid (pH 4.5) was added. Then, a solid phase extraction procedure was performed with Oasis MAX mixed polymer phase cartridges, preconditioned with 2 mL of methanol and equilibrated with 2 mL of formic acid (0.02 M, pH 4.5). Samples were loaded onto the cartridges, and successive washings were performed using 2 mL of 2% (v/v) NH_3, 2 mL of a methanol:formic acid (0.02 M, pH 4.5) mixture (30:70), 2 mL of hexane, and 2 mL of a hexane:ethyl acetate mixture (70:30). Columns were dried for 5 min. The retained PhytoPs, NeuroPs, and IsoPs were collected following two elutions with 1 mL of a hexane:ethanol:acetic acid mixture (70:29.4:0.6). Samples were concentrated under nitrogen at 40°C for 30 min and reconstituted in 100 µL of mobile phase (solvent A, water with 0.1% formic acid; solvent B, acetonitrile:MeOH, 8:2 [v/v] with 0.1% formic acid; A/B ratio, 83:17) for injection. Isoprostanoids were separated as described earlier (Vigor et al., 2018). Mass spectrometry analyses were performed using an AB SCIEX QTRAP 5500 (Sciex Applied Biosystems). The ionization source was electrospray, operated in negative mode. The source voltage was kept at ×4.5 kV, and N_2 was used as the curtain gas. Detection of the fragmentation ion products from each PhytoP, NeuroP, and IsoP deprotonated molecule $[M–H]^-$ was performed in multiple reaction monitoring mode. Quantification of PhytoPs, NeuroPs, and IsoPs was carried out by measuring the area under the specific peak using MultiQuant 3.0 software (Sciex Applied Biosystems). Area values were normalized to the cell concentration. The concentration of the analytes was obtained by calibration curves calculated by the area ratio of the analytes and the isoprostanoid internal standard (Vigor et al., 2018).

Genomic Sequence Analyses

The search for genes coding for potential homologs of reference sequences characterized in other organisms, such as human or Arabidopsis (*Arabidopsis thaliana*), was achieved using BLAST (Altschul et al., 1990). Reference genes were selected in the Uniprot (https://www.uniprot.org/) and TAIR (https://www.arabidopsis.org/) databases. Parameters selected for BLAST searches were as follows: scoring matrix, Blosum62; penalty for gap opening, 11; penalty for gap extension, 1; and with a filter for low-complexity regions. The last version of the *P. tricornutum* genome was obtained via the Ensembl portal (http://protists.ensembl.org/Phaeodactylum_tricornutum).

Statistical Analyses

Analyses were performed in biological triplicates. Statistical analyses were achieved using GraphPad Prism software 6.07 (GraphPad Software). One-way and two-way ANOVA followed by Dunnett's posthoc test were carried out. The difference between groups was considered significant at $P \leq 0.05$.

Supplemental Data

The following supplemental materials are available.

Supplemental Figure S1. Examples of enzymatic prostanoids from plants and animals and of nonenzymatic isoprostanoids.

Supplemental Figure S2. Effect of H_2O_2 on *P. tricornutum* cells after 48 h of treatment.

ACKNOWLEDGMENTS

We thank Amandine Rocher, Valerie Bultel, and Alexandre Guy for isoprostanoid analyses.

Received July 30, 2018; accepted September 11, 2018; published September 20, 2018.

LITERATURE CITED

Abida H, Dolch LJ, Meï C, Villanova V, Conte M, Block MA, Finazzi G, Bastien O, Tirichine L, Bowler C, (2015) Membrane glycerolipid remodeling triggered by nitrogen and phosphorus starvation in *Phaeodactylum tricornutum*. Plant Physiol **167**: 118–136

Allen AE, Laroche J, Maheswari U, Lommer M, Schauer N, Lopez PJ, Finazzi G, Fernie AR, Bowler C (2008) Whole-cell response of the pennate diatom Phaeodactylum tricornutum to iron starvation. Proc Natl Acad Sci USA **105**: 10438–10443

Allorent G, Courtois F, Chevalier F, Lerbs-Mache S (2013) Plastid gene expression during chloroplast differentiation and dedifferentiation into non-photosynthetic plastids during seed formation. Plant Mol Biol **82**: 59–70

Altschul SF, Gish W, Miller W, Myers EW, Lipman DJ (1990) Basic local alignment search tool. J Mol Biol **215**: 403–410

Andreou A, Feussner I (2009) Lipoxygenases: structure and reaction mechanism. Phytochemistry **70**: 1504–1510

Andreou A, Brodhun F, Feussner I (2009) Biosynthesis of oxylipins in non-mammals. Prog Lipid Res **48**: 148–170

Arao T, Yamada M (1994) Biosynthesis of polyunsaturated fatty acids in the marine diatom *Phaeodactylum tricornutum*. Phytochemistry **35**: 1177–1181

Arao T, Kawaguchi A, Yamada M (1987) Positional distribution of fatty acids in lipids of the marine diatom Phaeodactylum tricornutum. Phytochemistry **26**: 2573–2576

Arao T, Sakaki T, Yamada M (1994) Biosynthesis of polyunsaturated lipids in the diatom Phaeodactylum tricornutum. Phytochemistry **36**: 629–635

Bailey AP, Koster G, Guillermier C, Hirst EM, MacRae JI, Lechene CP, Postle AD, Gould AP (2015) Antioxidant role for lipid droplets in a stem cell niche of Drosophila. Cell **163**: 340–353

Barbosa M, Collado-González J, Andrade PB, Ferreres F, Valentão P, Galano JM, Durand T, Gil-Izquierdo Á (2015) Nonenzymatic α-linolenic acid derivatives from the sea: macroalgae as novel sources of phytoprostanes. J Agric Food Chem **63**: 6466–6474

Benoiston AS, Ibarbalz FM, Bittner L, Guidi L, Jahn O, Dutkiewicz S, Bowler C (2017) The evolution of diatoms and their biogeochemical functions. Philos Trans R Soc Lond B Biol Sci **372**: 372

Blée E (1998) Phytooxylipins and plant defense reactions. Prog Lipid Res **37**: 33–72

Blée E (2002) Impact of phyto-oxylipins in plant defense. Trends Plant Sci **7**: 315–322

Buchan A, LeCleir GR, Gulvik CA, González JM (2014) Master recyclers: features and functions of bacteria associated with phytoplankton blooms. Nat Rev Microbiol **12**: 686–698

Burch AR, Franz AK (2016) Combined nitrogen limitation and hydrogen peroxide treatment enhances neutral lipid accumulation in the marine diatom Phaeodactylum tricornutum. Bioresour Technol **219**: 559–565

Buseman CM, Tamura P, Sparks AA, Baughman EJ, Maatta S, Zhao J, Roth MR, Esch SW, Shah J, Williams TD, (2006) Wounding stimulates the accumulation of glycerolipids containing oxophytodienoic acid and dinor-oxophytodienoic acid in Arabidopsis leaves. Plant Physiol **142**: 28–39

Butler WL, Kitajima M (1975) Fluorescence quenching in photosystem II of chloroplasts. Biochim Biophys Acta **376**: 116–125

Casotti R, Mazza S, Brunet C, Vantrepotte V, Ianora A, Miralto A (2005) Growth inhibition and toxicity of the diatom aldehyde 2-trans,4-trans-decadienal on Thalassiosira weissflogii (Bacillariophyceae). J Phycol **41**: 7–20

Collado-González J, Durand T, Ferreres F, Medina S, Torrecillas A, Gil-Izquierdo Á (2015) Phytoprostanes. Lipid Technol **27**: 127–130

Collins JR, Edwards BR, Fredricks HF, Van Mooy BAS (2016) LOBSTAHS: an adduct-based lipidomics strategy for discovery and identification of oxidative stress biomarkers. Anal Chem **88**: 7154–7162

Conte M, Lupette J, Seddiki K, Meï C, Dolch LJ, Gros V, Barette C, Rébeillé F, Jouhet J, Maréchal E (2018) Screening for biologically annotated drugs that trigger triacylglycerol accumulation in the diatom Phaeodactylum. Plant Physiol **177**: 532–552

Cooksey KE, Guckert JB, Williams SA, Callis PR (1987) Fluorometric determination of the neutral lipid content of microalgal cells using Nile Red. J Microbiol Methods **6**: 333–345

Curien G, Flori S, Villanova V, Magneschi L, Giustini C, Forti G, Matringe M, Petroutsos D, Kuntz M, Finazzi G (2016) The water to water cycles in microalgae. Plant Cell Physiol **57**: 1354–1363

Demé B, Cataye C, Block MA, Maréchal E, Jouhet J (2014) Contribution of galactoglycerolipids to the 3-dimensional architecture of thylakoids. FASEB J **28**: 3373–3383

Di Dato V, Orefice I, Amato A, Fontanarosa C, Amoresano A, Cutignano A, Ianora A, Romano G (2017) Animal-like prostaglandins in marine microalgae. ISME J **11**: 1722–1726

Dolch LJ, Maréchal E (2015) Inventory of fatty acid desaturases in the pennate diatom Phaeodactylum tricornutum. Mar Drugs **13**: 1317–1339

Dolch LJ, Lupette J, Tourcier G, Bedhomme M, Collin S, Magneschi L, Conte M, Seddiki K, Richard C, Corre E, (2017) Nitric oxide mediates nitrite-sensing and acclimation and triggers a remodeling of lipids. Plant Physiol **175**: 1407–1423

Durand T, Guy A, Henry O, Roland A, Bernad S, El Fangour S, Vidal JP, Rossi JC (2004) Total syntheses of iso-, neuro- and phytoprostanes: new insight in lipid chemistry. Chem Phys Lipids **128**: 15–33

El Fangour S, Guy A, Vidal JP, Rossi JC, Durand T (2005) A flexible synthesis of the phytoprostanes B1 type I and II. J Org Chem **70**: 989–997

Falciatore A, d'Alcalà MR, Croot P, Bowler C (2000) Perception of environmental signals by a marine diatom. Science **288**: 2363–2366

Feussner I, Wasternack C (2002) The lipoxygenase pathway. Annu Rev Plant Biol **53**: 275–297

Funk CD (2001) Prostaglandins and leukotrienes: advances in eicosanoid biology. Science **294**: 1871–1875

Galano JM, Lee YY, Oger C, Vigor C, Vercauteren J, Durand T, Giera M, Lee JC (2017) Isoprostanes, neuroprostanes and phytoprostanes: an overview of 25 years of research in chemistry and biology. Prog Lipid Res **68**: 83–108

Gallina AA, Palumbo A, Casotti R (2016) Oxidative pathways in response to polyunsaturated aldehydes in the marine diatom Skeletonema marinoi (Bacillariophyceae). J Phycol **52**: 590–598

Gerecht A, Romano G, Ianora A, d'Ippolito G, Cutignano A, Fontana A (2011) Plasticity of oxylipin metabolism among clones of the marine diatom Skeletonema marinoi (Bacillariophyceae). J Phycol **47**: 1050–1056

Guy A, Oger C, Heppekausen J, Signorini C, De Felice C, Fürstner A, Durand T, Galano JM (2014) Oxygenated metabolites of n-3 polyunsaturated fatty acids as potential oxidative stress biomarkers: total synthesis of 8-F3t-IsoP, 10-F4t-NeuroP and [D4]-10-F4t-NeuroP. Chemistry **20**: 6374–6380

Guy A, Flanagan S, Durand T, Oger C, Galano JM (2015) Facile synthesis of cyclopentenone B1- and L1-type phytoprostanes. Front Chem **3**: 41

Ibrahim A, Mbodji K, Hassan A, Aziz M, Boukhettala N, Coëffier M, Savoye G, Déchelotte P, Marion-Letellier R (2011a) Anti-inflammatory and anti-angiogenic effect of long chain n-3 polyunsaturated fatty acids in intestinal microvascular endothelium. Clin Nutr **30**: 678–687

Ibrahim A, Schütz AL, Galano JM, Herrfurth C, Feussner K, Durand T, Brodhun F, Feussner I (2011b) The alphabet of galactolipids in *Arabidopsis thaliana*. Front Plant Sci **2**: 95

Imbusch R, Mueller MJ (2000) Formation of isoprostane F(2)-like compounds (phytoprostanes F(1)) from α-linolenic acid in plants. Free Radic Biol Med **28**: 720–726

Jahn U, Galano JM, Durand T (2010) A cautionary note on the correct structure assignment of phytoprostanes and the emergence of a new prostane ring system. Prostaglandins Leukot Essent Fatty Acids **82**: 83–86

Janssen LJ (2001) Isoprostanes: an overview and putative roles in pulmonary pathophysiology. Am J Physiol Lung Cell Mol Physiol **280**: L1067–L1082

Johnson X, Vandystadt G, Bujaldon S, Wollman FA, Dubois R, Roussel P, Alric J, Béal D (2009) A new setup for in vivo fluorescence imaging of photosynthetic activity. Photosynth Res **102**: 85–93

Jouhet J, Maréchal E, Bligny R, Joyard J, Block MA (2003) Transient increase of phosphatidylcholine in plant cells in response to phosphate deprivation. FEBS Lett **544**: 63–68

Jouhet J, Lupette J, Clerc O, Magneschi L, Bedhomme M, Collin S, Roy S, Maréchal E, Rébeillé F (2017) LC-MS/MS versus TLC plus GC methods: consistency of glycerolipid and fatty acid profiles in microalgae and higher plant cells and effect of a nitrogen starvation. PLoS ONE **12**: e0182423

Li W, Gao K, Beardall J (2012) Interactive effects of ocean acidification and nitrogen-limitation on the diatom Phaeodactylum tricornutum. PLoS ONE **7**: e51590

Loeffler C, Berger S, Guy A, Durand T, Bringmann G, Dreyer M, von Rad U, Durner J, Mueller MJ (2005) B1-phytoprostanes trigger plant defense and detoxification responses. Plant Physiol **137**: 328–340

Long EK, Murphy TC, Leiphon LJ, Watt J, Morrow JD, Milne GL, Howard JR, Picklo MJ Sr (2008) Trans-4-hydroxy-2-hexenal is a neurotoxic product of docosahexaenoic (22:6; n-3) acid oxidation. J Neurochem **105**: 714–724

Longini M, Belvisi E, Proietti F, Bazzini F, Buonocore G, Perrone S (2017) Oxidative stress biomarkers: establishment of reference values for isoprostanes, AOPP, and NPBI in cord blood. Mediators Inflamm **2017**: 1758432

Lupette J, Maréchal E (2018) Phytoplankton glycerolipids, challenging but promising prospects from biomedicine to green chemistry and biofuels. *In* **S La Barre, SS Bates**, eds, Blue Technologies: Production and Use of Marine Molecules. Wiley VCH, Weinheim, Germany, pp 191–215

Mallick N, Mohn FH (2000) Reactive oxygen species: response of algal cells. J Plant Physiol **157**: 183–193

McCarthy JK, Smith SR, McCrow JP, Tan M, Zheng H, Beeri K, Roth R, Lichtle C, Goodenough U, Bowler CP, (2017) Nitrate reductase knockout uncouples nitrate transport from nitrate assimilation and drives repartitioning of carbon flux in a model pennate diatom. Plant Cell **29**: 2047–2070

Milne GL, Yin H, Hardy KD, Davies SS, Roberts LJ II (2011) Isoprostane generation and function. Chem Rev **111**: 5973–5996

Miralto A, Barone G, Romano G, Poulet SA, Ianora A, Russo GL, Buttino I, Mazzarella G, Laabir M, Cabrini M, (1999) The insidious effect of diatoms on copepod reproduction. Nature **402**: 173–176

Misra AN, Misra M, Singh R (2012) Chlorophyll fluorescence in plant biology. *In* **AN Misra**, ed, Biophysics. InTech, Rijeka, Croatia, pp 171–192

Montuschi P, Barnes PJ, Roberts LJ II (2004) Isoprostanes: markers and mediators of oxidative stress. FASEB J **18**: 1791–1800

Morrow JD, Hill KE, Burk RF, Nammour TM, Badr KF, Roberts LJ II (1990) A series of prostaglandin F2-like compounds are produced in vivo in humans by a non-cyclooxygenase, free radical-catalyzed mechanism. Proc Natl Acad Sci USA **87**: 9383–9387

Morrow JD, Awad JA, Boss HJ, Blair IA, Roberts LJ II (1992) Non-cyclooxygenase-derived prostanoids (F2-isoprostanes) are formed in situ on phospholipids. Proc Natl Acad Sci USA **89**: 10721–10725

Mueller S, Hilbert B, Dueckershoff K, Roitsch T, Krischke M, Mueller MJ, Berger S (2008) General detoxification and stress responses are mediated by oxidized lipids through TGA transcription factors in *Arabidopsis*. Plant Cell **20**: 768–785

Mullineaux PM, Exposito-Rodriguez M, Laissue PP, Smirnoff N (2018) ROS-dependent signalling pathways in plants and algae exposed to high light: comparisons with other eukaryotes. Free Radic Biol Med **122**: 52–64

Nourooz-Zadeh J, Liu EHC, Anggård E, Halliwell B (1998) F4-isoprostanes: a novel class of prostanoids formed during peroxidation of docosahexaenoic acid (DHA). Biochem Biophys Res Commun **242**: 338–344

Oger C, Bultel-Poncé V, Guy A, Balas L, Rossi JC, Durand T, Galano JM (2010) The handy use of Brown's P2-Ni catalyst for a skipped diyne deuteration: application to the synthesis of a [D4]-labeled F4t-neuroprostane. Chemistry **16**: 13976–13980

Parchmann S, Mueller MJ (1998) Evidence for the formation of dinor isoprostanes E1 from α-linolenic acid in plants. J Biol Chem **273**: 32650–32655

Popko J, Herrfurth C, Feussner K, Ischebeck T, Iven T, Haslam R, Hamilton M, Sayanova O, Napier J, Khozin-Goldberg I, (2016) Metabolome analysis reveals betaine lipids as major source for triglyceride formation, and the accumulation of sedoheptulose during nitrogen-starvation of Phaeodactylum tricornutum. PLoS ONE **11**: e0164673

Roberts LJ II, Montine TJ, Markesbery WR, Tapper AR, Hardy P, Chemtob S, Dettbarn WD, Morrow JD (1998) Formation of isoprostane-like compounds (neuroprostanes) in vivo from docosahexaenoic acid. J Biol Chem **273**: 13605–13612

Roháček K, Bertrand M, Moreau B, Jacquette B, Caplat C, Morant-Manceau A, Schoefs B (2014) Relaxation of the non-photochemical chlorophyll fluorescence quenching in diatoms: kinetics, components and mechanisms. Philos Trans R Soc Lond B Biol Sci **369**: 20130241

Roy J, Galano JM, Durand T, Le Guennec JY, Lee JC (2017) Physiological role of reactive oxygen species as promoters of natural defenses. FASEB J **31**: 3729–3745

Sattler SE, Mène-Saffrané L, Farmer EE, Krischke M, Mueller MJ, DellaPenna D (2006) Nonenzymatic lipid peroxidation reprograms gene expression and activates defense markers in *Arabidopsis* tocopherol-deficient mutants. Plant Cell **18**: 3706–3720

Scala S, Bowler C (2001) Molecular insights into the novel aspects of diatom biology. Cell Mol Life Sci **58**: 1666–1673

Simionato D, Block MA, La Rocca N, Jouhet J, Maréchal E, Finazzi G, Morosinotto T (2013) The response of Nannochloropsis gaditana to nitrogen starvation includes de novo biosynthesis of triacylglycerols, a decrease of chloroplast galactolipids, and reorganization of the photosynthetic apparatus. Eukaryot Cell **12**: 665–676

Strassburg K, Huijbrechts AM, Kortekaas KA, Lindeman JH, Pedersen TL, Dane A, Berger R, Brenkman A, Hankemeier T, van Duynhoven J, (2012) Quantitative profiling of oxylipins through comprehensive LC-MS/MS analysis: application in cardiac surgery. Anal Bioanal Chem **404**: 1413–1426

Taddei L, Stella GR, Rogato A, Bailleul B, Fortunato AE, Annunziata R, Sanges R, Thaler M, Lepetit B, Lavaud J, (2016) Multisignal control of expression of the LHCX protein family in the marine diatom Phaeodactylum tricornutum. J Exp Bot **67**: 3939–3951

Thoma I, Loeffler C, Sinha AK, Gupta M, Krischke M, Steffan B, Roitsch T, Mueller MJ (2003) Cyclopentenone isoprostanes induced by reactive oxygen species trigger defense gene activation and phytoalexin accumulation in plants. Plant J **34**: 363–375

Vardi A, Formiggini F, Casotti R, De Martino A, Ribalet F, Miralto A, Bowler C (2006) A stress surveillance system based on calcium and nitric oxide in marine diatoms. PLoS Biol **4**: e60

Vigor C, Reversat G, Rocher A, Oger C, Galano JM, Vercauteren J, Durand T, Tonon T, Leblanc C, Potin P (2018) Isoprostanoids quantitative profiling of marine red and brown macroalgae. Food Chem **268**: 452–462

Vu HS, Tamura P, Galeva NA, Chaturvedi R, Roth MR, Williams TD, Wang X, Shah J, Welti R (2012) Direct infusion mass spectrometry of oxylipin-containing Arabidopsis membrane lipids reveals varied patterns in different stress responses. Plant Physiol **158**: 324–339

Warring SD, Dou Z, Carruthers VB, McFadden GI, van Dooren GG (2014) Characterization of the chloroquine resistance transporter homologue in Toxoplasma gondii. Eukaryot Cell **13**: 1360–1370

Wenk MR (2010) Lipidomics: new tools and applications. Cell **143**: 888–895